A Navigational System for Quadcopter Remote Inspection of Offshore Substations

Elisabeth Welburn*, Hassan Hakim Khalili†, Ananya Gupta‡, Joaquin Carrasco§ and Simon Watson¶
School of Electrical and Electronic Engineering
The University of Manchester, Manchester, UK M14 9PL
*Email: Elisabeth.Welburn@manchester.ac.uk
† Email: Hassan.Hakimkhalili@manchester.ac.uk
‡ Email: Ananya.Gupta@manchester.ac.uk
§ Email: Joaquin.Carrasco@manchester.ac.uk
¶ Email: Simon.Watson@manchester.ac.uk

***Abstract*—Effective and safe maintenance of offshore infrastructure is hampered by its remote location. Robotic inspection can provide a retrofit solution, improving safety for human personnel by removing them from a potentially hazardous environment, and also reduce operational costs. There are three primary challenges for navigation around an offshore substation: low visibility, high electromagnetic fields and the absence of Global Positioning System (GPS) signals. This paper details a navigational system that enables Unmanned Aerial Vehicles (UAVs) to operate within a dark and GPS-denied environment.**

Keywords–Robotics In Hazardous Fields; Aerial Robotics; SLAM; Sensor-based Control.

I. INTRODUCTION

The remote inspection and asset management of offshore wind farms and the connection to shore will be worth up to 2 billion pounds annually by 2025. However, current methods of inspection are dangerous for human personnel and introduce high costs for the industry as a whole [1].

Currently, Supervisory Control and Data Acquisition (SCADA) systems and thermal imaging inspections are being used in data management to inform substation operations and maintenance. However, the limited number of qualified inspectors coupled with the high demand leads to common unexpected failures. Automation could potentially alleviate this by increasing inspection frequency and standardizing procedures [2].

Robotic inspection platforms have the potential to ensure the maintenance of vital infrastructure, reducing associated expenditure and hazards [1]. However, this endeavour presents unique challenges that must be overcome for it to become a viable commercial method. Considering the offshore substation environment in the context of a navigational system, the inherently symmetrical nature coupled with the occlusion of GPS signal may attribute to difficulty ascertaining an accurate estimation of the robot's global 6 Degree of Freedom (DoF) pose. The high electromagnetic fields necessitate the use of shielding, limiting external sensor hardware [3]. The presence of high electromagnetic fields could potentially interfere with the nominal operation of the propulsion motors [4]. To circumvent this, the use of a magnetometer within the proposed navigational system will be neglected. Moreover, the sensor payload must also be minimal to extend battery life, facilitating the implementation of autonomous capabilities in this remote location. Also, the absence of visible light limits the use of vision-based odometry.

Three levels of autonomy can be defined: pure tele-operation, safe-guarded tele-operation and autonomous navigation [5]. The navigational system presented within this paper provides a method of remote tele-operation. However, the aim is to extend this system to full autonomy in the future with more sophisticated obstacle avoidance capabilities that account for the electromagnetic fields.

This paper presents a navigational system for UAVs to operate inside a High Voltage Direct Current (HVDC) valve hall. The quadcopter is equipped with two 2D Light Detection and Ranging (LiDAR) devices that are mounted perpendicularly to each other, the combination of which provides a 3D estimation of the robot pose. However, this estimation is, in part, based upon relative movement of the surrounding landmarks between frames and so is subject to a certain amount of drift. This is further exacerbated by the repetitive and symmetrical nature of these landmarks. To remedy this, the implementation of Quick Response (QR) codes were investigated as global reference points to correct for this accumulated error. Sensor fusion was accomplished with the use of an Extended Kalman Filter (EKF).

The remainder of this paper is structured as follows: Section II of this paper will consider related works and Section III will detail the system architecture, while Section IV will analyse the collated results and several conclusions will be drawn concerning further extensions of this work and the viability of this system within industry.

II. RELATED WORK

To inform system design, the state-of-the-art navigational techniques were considered for UAVs as well as ground vehicles, with the view of adapting these methods for UAV navigation of a GPS-denied and dark environment.

A. Current Navigational Techniques

In [6], an autonomous navigational system was developed for a ground vehicle deployed within a GPS-denied greenhouse. This system used the Hector Simultaneous Localisation and Mapping (SLAM) Robot Operating System (ROS) package, that is also used within this system, and combined this with a potential fields path planning algorithm. Structural changes due to the growth of crops were accounted in the path planning algorithm while being safe to operate in the presence of humans. This is reminiscent of faults occurring and causing a fluctuation of electromagnetic fields inside the HVDC valve hall environment, changing the required clearances to maintain nominal operation of the UAV.

In [7], a UAV was deployed into a GPS-denied, dark tunnel where a perception system comprising of a near-infra-red

 ISBN: 978-1-61208-712-2

stereo camera, flashing LEDs, inertial sensors, and a 3D depth sensor to derive the geometry of the environment. A horizon-based planner accounted for the system's uncertainty during mission execution and generated collision-free exploration paths. However, the environment here was unknown and static, whereas the valve hall geometry is known and faults within the racks can cause a fluctuation of the electromagnetic fields.

In [2], a robot transverses substations with the use of a rail system and collects IR and visible images, positioning, time and component description and transmits this, as well as energy, to a control centre with the use of the rails. This mitigates faults caused by intermediate electromagnetic interference between the robot and the control centre. Also, magnetic references on the rails negate the need for markings implemented onto the substation infrastructure. Also, the use of the commercial voltage for Brazil facilitates installation in other locations. However, the rail-based robot requires the installation of an extensive rail system in existing substations to operate [2]. The system proposed within this paper provides a retro-fit solution that could potentially accomplish the same task.

B. Vision-Based Odometry Techniques

The dark nature of the valve hall restricts the perception within the visible spectrum. However, a Near-Infrared (NIR) camera will be fitted to the drone for fault detection purposes and also a LED spotlight can provide limited ambient lighting in the immediate vicinity.

In general, though visual odometry is useful for local position control and stability, these methods often suffer from long-term drifts and are not suitable for building large-scale maps [8]. RGB-D cameras provide both a colour image and per-pixel depth estimates and are prominent within mobile robotic platforms due to their richness of the data collected coupled with their reducing cost. In [8], a system for the navigation of a micro-air vehicle within a cluttered, GPS-denied indoor environments with the use of an on-board RGB-D camera and an Inertial Measurement Unit (IMU) was developed. This system periodically corrected for the drift present within the local state estimation based upon visual odometry with results from the RGB-D mapping algorithm [9]. However, this system was unsuitable for real-time situations as the loop closing and SLAM algorithms were not sufficiently fast to be run on an on-board processor.

The use of Quick Response codes within absolute localisation methods for indoor mobile robots is widespread due to their large data storage capabilities, small size, low cost and simple implementation. A possible issue with their use is that the recognition rate is reduced if the QR code is small within the camera's field of view or the robot moves too fast. Considering this application in real-time, the processing resources are sufficiently low to enable use of the QR codes, as it was found within [10], that the time taken to calculate the relative position of the robot was between 20 to 30 ms.

Within [10], an industrial camera was mounted onto a mobile ground robot pointing upwards in order to identify QR codes mounted to the ceiling. Meanwhile, a laser range-finder was used for object detection as well as the construction of a 2D map with the use of a Rao-Blackwellized particle filter. The Dijkstra algorithm, as well as the Dyanmic Window Approach were used to implement both local and global path planning capabilities [10]. However, this system is not usable in situations where the QR codes were occluded from the camera's field of view due to sheltering obstacles or ambient light. Odometry data was used to compensate for the drift occurring within the short time interval travelling between the QR codes, whereby the error accumulation was mitigated with the use of additional sensor inputs [10].

In [11], a tailored extended H_∞ filter (EHF) was implemented. This filter fused both odometry and gyroscope data with pose estimates based upon QR code landmarks. However, this method is more computationally expensive compared to an EKF, taking longer to converge on an accurate estimate [11], which is paramount when instructing real-time control as in this scenario.

III. System Architecture

Within this section, the architecture of the navigational system as depicted in Figure 1 is discussed.

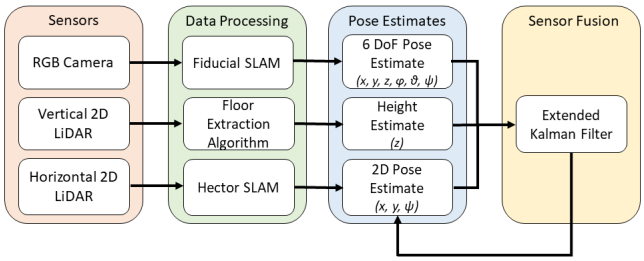

Figure 1. Software Architecture for the Proposed Navigational System.

A. Mobile Robotic Platform

The quadcopter utilised for the proof-of-concept system is the Hector quadrotor Robot Operating System (ROS) package [12] due to its pre-existing and well-documented integration with the Gazebo simulator. The visual geometry was written within COLLADA format and the collision geometry was modelled as a STL mesh. A low polygon count reduced the demand from rendering the model, allowing simulations to be ran at a higher percentage of real-time. The propellers were represented by actuator discs to facilitate the maintenance of boundary conditions [12]. The hector quadrotor is depicted below in Figure 2.

Figure 2. The Hector quadrotor rendered within the Gazebo simulator. Image taken from [12].

The CAD model of an offshore substation, as shown in Figure 3, with the correct clearances as the real-time environment was constructed and used to collate results.

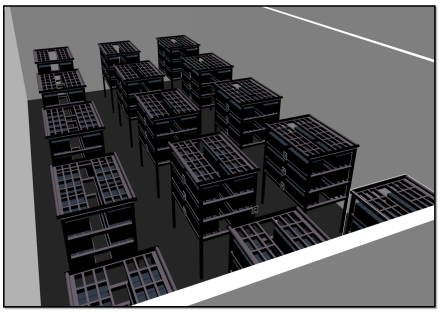

Figure 3. CAD model of the HVDC valve hall

B. 2D SLAM Algorithm

Low-cost laser range-finders are prevalent in autonomous robot applications due to their low price and ability to trace terrains and structures in the contiguous area, while consuming relatively little power [13].

In the proposed system, two Hokuyo utm-30lx LiDARs were mounted perpendicularly to each other. It was assumed that the z-axis was out-of-plane relative to the ground plane and the x-axis was pointing in the forward direction of the quadcopter. The horizontal, planar LiDAR was used within the 2D SLAM algorithm to construct a map of the surroundings.

A ROS node, Hector Mapping [14], was selected as the 2D SLAM algorithm, of which the only requirement was a high frequency laser scanner, such as the Hokuyo utm-30lx LiDAR in this scenario.

C. Floor Extraction

For height estimation and greater spatial understanding, a secondary LiDAR was mounted, perpendicular to the primary LiDAR, onto the underside of Hector quadrotor. The vertical LiDAR produced a 2D vertical laser scan of the environment. A split-and-merge algorithm [15] was then implemented to differentiate the walls and floor using the relative angle of the incident laser endpoints. The roll and pitch recorded by the EKF was processed and the calculated relative angles of the identified line segments were rotated to avoid falsely recognising the walls as the floor during operation.

A laser pointing vertically downwards was also considered as the method of height estimation, however this is a less robust method than the aforementioned secondary LiDAR. This is because if the quadrotor turned near the boundaries of the space, the singular laser point could potentially rotate to be incidental on walls or substation racks. This could be mitigated with the use of fusion with the orientation from the IMU device to account for the laser rotation. However, IMU data suffers from drift and so a secondary LiDAR was used in the implementation to provide more information of the transformation of the laser scan points relative to the quadrotor.

D. QR Codes as Global Landmarks

Vision-based odometry is generally computationally intensive and also suffers from robustness under varying lighting conditions [11]. However, in this scenario there is an absence of visible light and so ambient light levels are constant. Also, vision-based odometry was implemented with the view to periodically correct for drift in the 2D SLAM algorithm pose estimations.

A FLIR One Near-Infrared (NIR) camera of a spectral range between 8 - 14 μm will be utilised to enable simultaneous QR code detection and faults within the infrared spectrum. An infrared LED emitting light between 750 - 950 nm will be mounted on top of the camera, illuminating the proximal field of view. However, for the purposes of this simulation, a generic camera is created within a virtual world lit by ambient lighting to ensure an accurate estimation of the nominal accuracy of the vision-based odometry.

The QR codes were generated with the use of the open-source library, arUco markers. These were then placed on the racks within the virtual substation environment at regular intervals. The ROS package, fiducial SLAM [16], was used to both identify the unique identifier of the QR code as well as produce a 6 DoF pose estimation of the drone using the known global poses of the QR codes.

The QR codes could potentially be used in two capacities during drone operation. Correct identification of a unique QR code indicates the drone is within the correct general vicinity of the rack. These could form the basis of a command interface to set the goal destination that determines the generated path. The unique identifiers of visible QR codes in the camera field of view are shown in Figure 3.

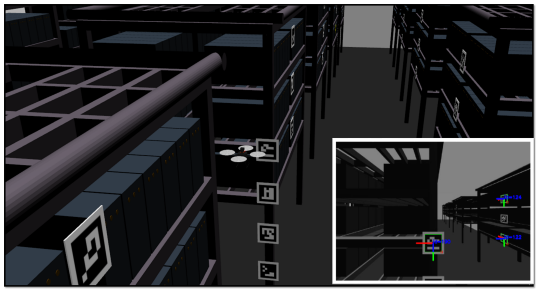

Figure 4. The virtual UAV inspecting a substation rack. Inset is the camera field of view.

Alternatively, the pose of the visible QR marker in a known location can be processed to output a 6 DoF pose estimation of the drone that could have been later fused with the other sensor measurements within the EKF. However, this was found to produce erroneous estimations of 6 DoF pose, as discussed later.

IV. SENSOR FUSION

Sensor fusion was necessary within this system to identify the optimal estimate of the UAVs pose. Considering the sensor measurements modelled in this section, $(x_s, y_s, z_s, \phi_s, \theta_s, \Psi_s)$ was produced from the 2D SLAM performed using the planar LiDAR, z from the height measurement using the perpendicular LiDAR and, finally, $(x, y, z, \phi, \theta, \Psi)$ was produced from the vision-based odometry system based upon QR codes visible to the on-board camera.

First, the orientation measurements must be converted from a quarternion in the local frame to Euler angles that are relative to the global frame. A function available within the ROS python library tf was used for this conversion. For the purposes of this system, the starting pose of the spawned robot

 ISBN: 978-1-61208-712-2

was assumed to be the global frame in terms of the way-point commands that were converted into command velocities. However, this coordinate frame was mapped onto the 2D occupancy grid constructed to utilise the A* path planning algorithm.

The measurements were taken at different unsynchronised rates. To accompany this, each sensor measurement was sampled with each new IMU measurement at a rate of 100 Hz. In this way, a sufficient sample rate was ensured.

Kalman filters are algorithms for the estimation of dynamic state variables by combining state predictions with measurements. For discrete systems, the future values of the state variables can be predicted using Kalman filters.

The EKF can overcome the linearity assumption of the Kalman Filter that both the motion model and sensor model are linear Gaussian [13]. Within this system, an extended Kalman filter was implemented, where the non-linearity is introduced with the continuously-variable rotation relative to the global frame.

For time-invariant systems, the function f computed the predicted state from the previous estimate, and the h function computed the output. The variables, w_k and v_k, represented the process and observation white noises, respectively, i. e.

$$x_{k+1} = f(x_k, u_k) + w_k \tag{1}$$
$$z_k = h(x_k) + v_k \tag{2}$$

The white noises w_k and v_k were assumed to be zero mean and covariances Q_k and R_k, respectively.

For the purposes of this Kalman filter, all variables were within the global frame. The values used for initialisation of the Kalman filter were the coordinates of spawning the robot model.

In the case of the Hector quadcopter, the state variables were updated with the use of inertial measurements from the IMU unit. The state vector, X, comprised of these state variables:

$$X = [x \quad y \quad z \quad \dot{x} \quad \dot{y} \quad \dot{z} \quad \phi \quad \theta \quad \Psi]^T \tag{3}$$

where x, y, z were the positions on the X, Y, and Z axes and ϕ was the roll, θ, the pitch and Ψ, the yaw of the quadrotor.

The global displacement, s, in each of the X, Y and Z axes was modelled using dead reckoning with the initial displacement, s_0, the rotation matrix that transforms between the body frame to the inertial frame, R, the initial velocity at the start of the time interval v_0, IMU acceleration within the IMU frame of reference, a, the gravitational constant, g, and the length of the time interval, t.

With some abuse of notation, this relationship was encapsulated in the dynamic matrix, f, that described how the state evolves to the next time step, as below:

$$f = \begin{bmatrix} s_0 + \dot{s}\triangle T + \frac{1}{2}R(a-g)\triangle T^2 \\ \dot{v}_0 + \triangle T\Big(R(a-g)\Big) \\ \alpha_0 + \triangle T\Theta \end{bmatrix}, \tag{4}$$

where Θ was the mapping of the angular velocities in the body frame (p, q, r) to the changes in the Euler angles within the inertial frame [17], e.g.

$$\Theta = \begin{bmatrix} 1 & \sin\phi\tan\theta & \cos\phi\tan\theta \\ 0 & \cos\phi & -\sin\phi \\ 0 & \frac{\sin\phi}{\cos\theta} & \frac{\cos\phi}{\cos\theta} \end{bmatrix}. \tag{5}$$

The measurement function, h, was given by

$$h = [x \quad y \quad z \quad \phi \quad \theta \quad \Psi]^T. \tag{6}$$

The linearisation of (1) provided the state transition matrix, F_k, by computing the Jacobian of the dynamic matrix f with respect to the state vector. Similarly, the observation matrix H_k was also be defined as the Jacobian of the measurement matrix, h with respect to the state vector.

The control inputs into the system were assumed to be the linear accelerations and the angular velocities as measured by the IMU, i.e.

$$u = \begin{bmatrix} \ddot{x} & \ddot{y} & \ddot{z} & \dot{\phi} & \dot{\theta} & \dot{\Psi} \end{bmatrix}^T \tag{7}$$

The time update of the EKF algorithm was given by

$$\hat{x}_{k|k-1} = f(x_{k-1}, u_{k-1}), \tag{8}$$
$$P_{k|k-1} = F_k P_{k-1|k-1} F_k^T + Q_k. \tag{9}$$

The measurement update steps were then computed to adjust the Kalman gain, K_k and to update the estimate with the actual measurement, z_k, and to update the error covariance, $P_{k|k}$. The measurement residual, $\widetilde{y}$ as well as the covariance residual, S_k were also calculated.

$$\widetilde{y}_k = z_k - h(\hat{x}_{k|k-1}) \tag{10}$$
$$S_k = H_k P_{k|k-1} H_k^T + R_k \tag{11}$$
$$K_k = P_{k|k-1} H_k^T S_k^{-1} \tag{12}$$
$$\hat{x}_{k|k} = \hat{x}_{k|k-1} + K_k \widetilde{y}_k \tag{13}$$
$$P_{k|k} = (I - K_k H_k) P_{k|k-1} \tag{14}$$

This method was less computationally expensive in comparison to other methods, such as the H_∞ filter (EHF) [11]. One of the drawbacks of an extended Kalman filter is that it is not an optimal estimator. Moreover, if the initial state vector is wrong, the filter will quickly diverge due to its linearisation. As a result, the EKF requires extensive tuning of these parameters.

V. Path Planning Algorithm

The final pose estimation from the EKF was fed into an A* path planning module [18]. The robot radius was considered greater than the nominal dimensions, ensuring clearances from the high electromagnetic fields present within the substation racks were maintained.

Prior to this, a 2D occupancy grid of the substation plan was constructed using the known dimensions of the CAD model. In terms of command way-points, height correction was performed first to adjust the drone to the specified goal height because of the largely constant geometry of the environment within the vertical plane. Then, an A* path planning algorithm was then used to generate the path shown in Figure 5 within the substation.

 ISBN: 978-1-61208-712-2

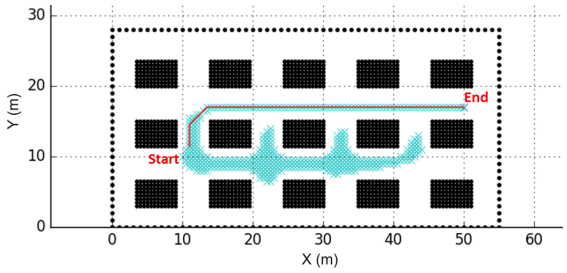

Figure 5. A 2D occupancy grid and path generated by the A* star algorithm

TABLE I. ERROR IN EKF OUTPUT

Global Axis	Distance Travelled (m)	Maximum Error (m)	Maximum Error (%)
x	39	0.65	1.67
y	5.5	0.3	5.45
z	5	0.015	0.3

This produced the optimal trajectory consisting of 0.5 m increments between the start position and goal position. After this, alterations to the orientation of the drone were made to enable 360 degree inspection.

VI. Results

To ascertain a baseline and compute the errors of the constituent algorithms, the standard deviations of each of the measurements were calculated. These standard deviations were then used as a baseline for tuning of the Q and R matrices within the EKF.

The pose estimation generated from the EKF during the mapped trajectory in Figure 5 was used to gauge the viability of the proposed navigational system. The IMU measurements, as well as the $hector\_mapping$ 2D pose and extracted floor height were fused by the EKF. The 3D position of the UAV is compared to the ground truth within Figure 6. The error present within the EKF output is tabulated in Table I. An error of 1.67% in the x-axis throughout the course of a twenty-minute mission is tolerable. However, an error of 5.45% in the y-axis is unsatisfactory and further tuning of the EKF is required to alleviate this. The height estimation algorithm was found to produce the least error, with a 0.3% throughout the length of the mission. The average battery life of a UAV is between ten to fifteen minutes, depending on payload and so these figures represent a probable overestimation of the drift present within the EKF.

The camera stream was also recorded, whereby visible QR codes unique identifiers were overlaid, as seen in Figure 4. The 6 DoF pose estimation from the visible QR codes was also collated to evaluate whether this data should be incorporated into the EKF. However, as can be seen by Figure 7, these pose estimations are extremely erratic and will not contribute to the overall stability of the EKF upon fusion.

The inaccurate 6 DoF pose estimation produced from the $fiducial\_slam$ could potentially be due to the 2D nature of the QR codes hindering precise depth perception. It also may be due to the monocular nature of the camera.

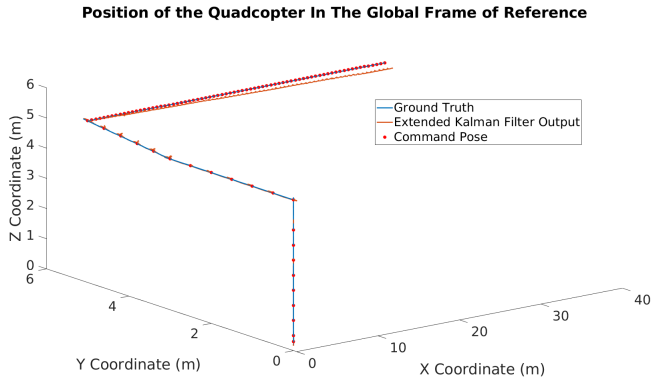

Figure 6. EKF pose estimation

Considering Figure 7, ultimately direct pose estimation from fiducial slam was not implemented within the EKF. However, the unique identifiers displayed within the camera stream could potentially facilitate inspection of substation racks by providing a visual verification of the current vicinity of the UAV.

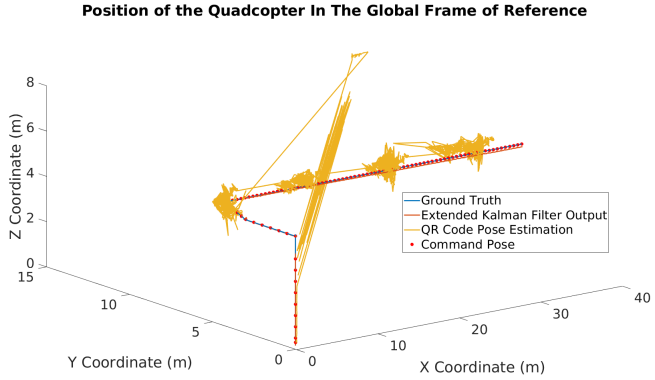

Figure 7. EKF pose estimation with the fiducial slam results

In summary, these set of results suggest that this framework could potentially be adapted for implementation into a real-world system.

VII. Conclusion

In conclusion, the proposed, proof-of-concept, navigational system paves the way for UAV navigation within dark, GPS-denied environments. This was acheived with the fusion of IMU data with processed LiDAR measurements. Possible mechanisms of correction via vision-based odometry upon the identification of QR codes within the environment were explored and it was concluded that though the QR codes provide visual cues of the drones current position they fail to act as reference points to generate an accurate 6 DoF pose. This system provides a retro-fit solution for the remote inspection of substations, merely requiring the careful placement of QR codes within the environment.

Future work includes the implementation of this navigational system onto a drone within an indoor, confined and dark environment. The computation and sensing required for

 ISBN: 978-1-61208-712-2

local position control will be performed on-board the vehicle, reducing the dependence on unreliable wireless links [8]. The path planning capabilities will also be expanded to account for the presence of electromagnetic fields with the implementation of a modified potential fields algorithm. Moreover, this system could potentially pave the way for the use of thermal imaging to identify faults within the substation infrastructure. This is advantageous in comparision to existing methods because it involves non-contact precision temperature measurements and non-destructive testing [5].

ACKNOWLEDGMENTS

This work was supported by the Holistic Operation and Maintenance for Energy from Offshore Wind Farms (HOME Offshore) project (EPSRC Grant Number: EP/P009743/1) and the Robotics and Artifical Intelligence for Nuclear (RAIN) project (EPSRC Grant Number: EP/R026084/1). The authors would like to thank both Dr. Andrew West and Dr. Thomas Wright of the University of Manchester for their continued support.

REFERENCES

[1] E. M. Barnes et al., "Technology Drivers in Windfarm Asset Management Position Paper," 2018, pp. 1–46.

[2] B. P. Silva et al., "On-rail solution for autonomous inspections in electrical substations," Infrared Physics & Technology, vol. 90, May 2018, pp. 53–58. [Online]. Available: https://www.sciencedirect.com/science/article/pii/S1350449517307247

[3] M. Heggo et al., "Evaluation and mitigation of high electrostatic fields on operation of aerial inspections vehicles in hvdc environments," in EERA DeepWind19, Jan 2019.

[4] M Heggo et al., "Evaluation and mitigation of offshore hvdc valve hall magnetic field impact on inspection quadcopter propulsion motors," in EERA DeepWind19, Jan 2019.

[5] P. Rea and E. Ottaviano, "Design and development of an Inspection Robotic System for indoor applications," Robotics and Computer-Integrated Manufacturing, vol. 49, Feb 2018, pp. 143–151. [Online]. Available: https://linkinghub.elsevier.com/retrieve/pii/S0736584517300613

[6] E. H. Harik, A. Korsaeth, E. H. C. Harik, and A. Korsaeth, "Combining Hector SLAM and Artificial Potential Field for Autonomous Navigation Inside a Greenhouse," Robotics, vol. 7, no. 2, May 2018, p. 22. [Online]. Available: http://www.mdpi.com/2218-6581/7/2/22

[7] C. Papachristos, S. Khattak, and K. Alexis, "Autonomous exploration of visually-degraded environments using aerial robots," in 2017 International Conference on Unmanned Aircraft Systems (ICUAS). IEEE, Jun 2017, pp. 775–780. [Online]. Available: http://ieeexplore.ieee.org/document/7991510/

[8] Huang et al., "Visual Odometry and Mapping for Autonomous Flight Using an RGB-D Camera." Springer, Cham, 2017, pp. 235–252. [Online]. Available: http://link.springer.com/10.1007/978-3-319-29363-914

[9] P. Henry, M. Krainin, E. Herbst, X. Ren, and D. Fox, "RGB-D Mapping: Using Depth Cameras for Dense 3D Modeling of Indoor Environments." Springer, Berlin, Heidelberg, 2014, pp. 477–491. [Online]. Available: http://link.springer.com/10.1007/978-3-642-28572-133

[10] H. Zhang, C. Zhang, W. Yang, and C.-Y. Chen, "Localization and navigation using QR code for mobile robot in indoor environment," in 2015 IEEE International Conference on Robotics and Biomimetics (ROBIO). IEEE, Dec 2015, pp. 2501–2506. [Online]. Available: http://ieeexplore.ieee.org/document/7419715/

[11] P. Nazemzadeh, D. Fontanelli, D. Macii, and L. Palopoli, "Indoor Localization of Mobile Robots Through QR Code Detection and Dead Reckoning Data Fusion," IEEE/ASME Transactions on Mechatronics, vol. 22, no. 6, Dec 2017, pp. 2588–2599. [Online]. Available: http://ieeexplore.ieee.org/document/8066377/

[12] J. Meyer, A. Sendobry, S. Kohlbrecher, U. Klingauf, and O. von Stryk, "Comprehensive simulation of quadrotor UAVs using ROS and gazebo," in Simulation, Modeling, and Programming for Autonomous Robots. Springer Berlin Heidelberg, 2012, pp. 400–411. [Online]. Available: https://doi.org/10.1007%2F978-3-642-34327-8_36

[13] W.-C. Jiang, M.-Y. Ju, Y.-J. Chen, and W.-C. Jiang, "Implementation of Odometry with EKF in Hector SLAM Methods," International Journal of Automation and Smart Technology, vol. 8, no. 1, Mar 2018, pp. 9–18. [Online]. Available: http://www.ausmt.org/index.php/AUSMT/article/view/1558

[14] "Hector mapping," accessed: 2019-05-09. [Online]. Available: \url{http://wiki.ros.org/hector_mapping}

[15] "Laser line extraction," accessed: 2019-05-09. [Online]. Available: https://github.com/kam3k/laser_line_extraction

[16] "Fiducial slam," accessed: 2019-05-09. [Online]. Available: https://github.com/UbiquityRobotics/fiducials

[17] T. I. Fossen, Handbook of Marine Craft Hydrodynamics and Motion Control. Chichester, UK: John Wiley & Sons, Ltd, Apr 2011. [Online]. Available: http://doi.wiley.com/10.1002/9781119994138

[18] "Pythonrobotics," accessed: 2019-05-09. [Online]. Available: https://github.com/AtsushiSakai/PythonRobotics

 ISBN: 978-1-61208-712-2